Guidance on the Use of Existing ASTM Polymer Testing Standards for ABS Parts Fabricated Using FFF

Arielle Miller[a,b], Celeste Brown[c], Grant Warner[d]

ABSTRACT

When evaluating the static mechanical performance of fused filament fabrication (FFF) polymers, researchers have conducted tensile testing using American Society for Testing Materials International (ASTM) D3039 rectangular test specimens and ASTM D638 Type I and Type IV dogbone test specimens. The choice of ASTM D638 versus ASTM D3039 test specimen geometry is usually based on the perceived susceptibility of the ASTM D638 test specimens to failure within the fillet radius. ASTM polymer and plastic tensile test standards define criteria for acceptably tested specimens as requiring failure inside the narrow length (i.e., ASTM D638) or outside of the grips (i.e., ASTM D3039) for the results to be considered acceptable. There has been limited published research regarding the selection of an ASTM test specimen geometry for FFF polymer materials. This study provides evidence-based guidance through the comparison of the mechanical performance and failure acceptance rates of ASTM D3039 and ASTM D638 test specimen geometries, fabricated using FFF acrylonitrile butadiene styrene (ABS). The purpose of the study is to provide guidance on the use of existing ASTM polymer testing standards for additively manufactured polymers. Results indicate there is an inherent benefit to using ASTM D3039 over ASTM D638 Type I and Type IV test specimens for tensile testing. ASTM D3039 test specimens provide the most consistent failure within the test specimen's gage length, which is attributed to the rectangular design of the test specimen. Results also indicated that, like traditionally manufactured polymer composites, there will be differences in the tensile test results (e.g., ultimate

[a] Department of Mechanical Engineering, Howard University, Washington, DC, USA; ORCID: 0000-0002-4320-0876
[b] Corresponding author: arielle.miller@bison.howard.edu
[c] Department of Mechanical Engineering, Howard University, Washington, DC, USA; ORCID: 0000-0002-5819-7948
[d] Department of Mechanical Engineering, Howard University, Washington, DC, USA

tensile strength, elastic modulus) based on the different cross-sectional areas of the test specimen geometries.

Keywords: tensile, FFF, ABS, additive manufacturing, polymer, standards

Introduction

In 2015, the National Institute of Standards and Technology (NIST) published a qualitative overview of American Society for Testing Materials International (ASTM) test methods considering their applicability to additively manufactured (AM) polymers[1], which included discussions on ASTM D638, *Standard Test Method for Tensile Properties of Plastics*[2] and ASTM D3039, *Standard Test Method for Tensile Properties of Polymer Matrix Composite Materials*[3]. ASTM D638 and ASTM D3039 do not explicitly exclude testing of fused filament fabrication (FFF) manufactured polymers; however, they have not been formally evaluated for FFF manufactured polymers. ASTM D638 Type I test specimens are provided in the D638 test method for testing reinforced composites[2]. ASTM D3039 rectangular test specimens are provided in the D3039 test method for testing only composite forms with "continuous or discontinuous" fibers that are "balanced and symmetric with the load."[3] ASTM D638 Type IV test specimens are recommended for testing non-rigid or semi-rigid plastics.[2] NIST has suggested either standard could be used "with guidance" for tensile testing of 3D printed polymers. NIST continues to study polymer-based additive manufacturing, focusing on improving measurement techniques, modeling, and product quality to help inform standard guidance.[4]

Even though ASTM D638 and ASTM D3039 are not explicitly written for testing 3D printed polymers, existing literature on FFF polymers typically references these standards as the basis for their test specimens and testing parameters. When evaluating the mechanical

performance of FFF polymers under static loading, most researchers have conducted tensile testing or modeling using ASTM D638 Type I (Figure 1) or Type IV (Figure 2) dogbone geometry test specimens or similar designs.[5-13] However, some researchers have chosen to perform tensile testing or modeling using the ASTM D3039 rectangular geometry test specimen (Figure 3).[13-18] The choice by researchers of the ASTM D3039 rectangular geometry instead of a ASTM D638 test specimen geometry has sometimes been based on the perceived susceptibility of the ASTM D638 test specimen geometries to failure within the radius.[14] In other cases, the perceived susceptibility of the ASTM D638 test specimen geometries to failure within the radius has driven researchers to modify the existing ASTM D638 dog bone geometry in an effort to remove that susceptibility.[19] The failure of ASTM D638 dog bone specimens at the fillet radius is a failure of the ASTM D638 acceptance criterion.[2] ASTM D638 requires that specimens which fail outside the narrow length be discarded and omitted from test results. Similarly, ASTM D3039 states that only rectangular test specimens that fail within the gage length shall be considered acceptable for inclusion in test results.[3] Since the ASTM D3039 rectangular specimens do not have a fillet radius, failure at or in the grip of the specimen qualifies as a failure to meet the acceptance criterion.

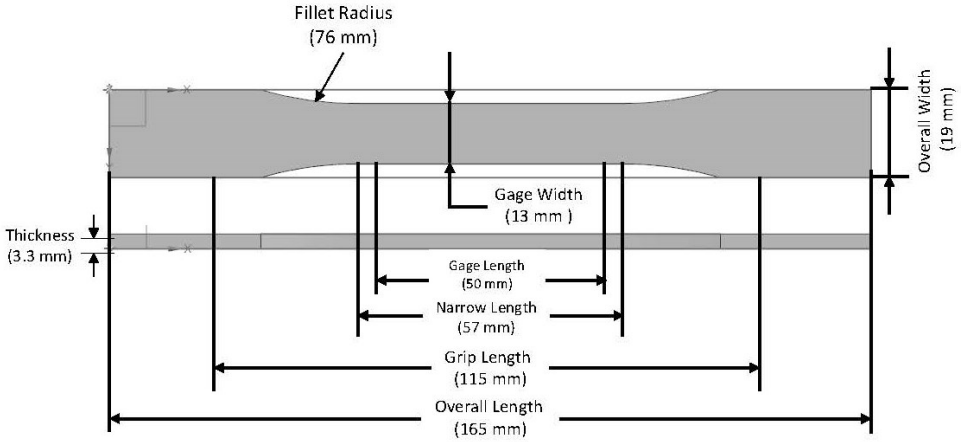

Figure 1. ASTM D638[2] Type I Test Specimen (Dimensions in mm)

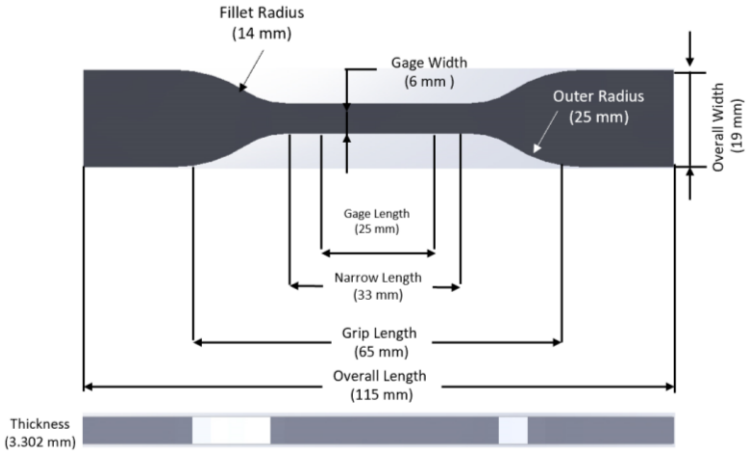

Figure 2. ASTM D638[2] Type IV Test Specimen (Dimensions in mm)

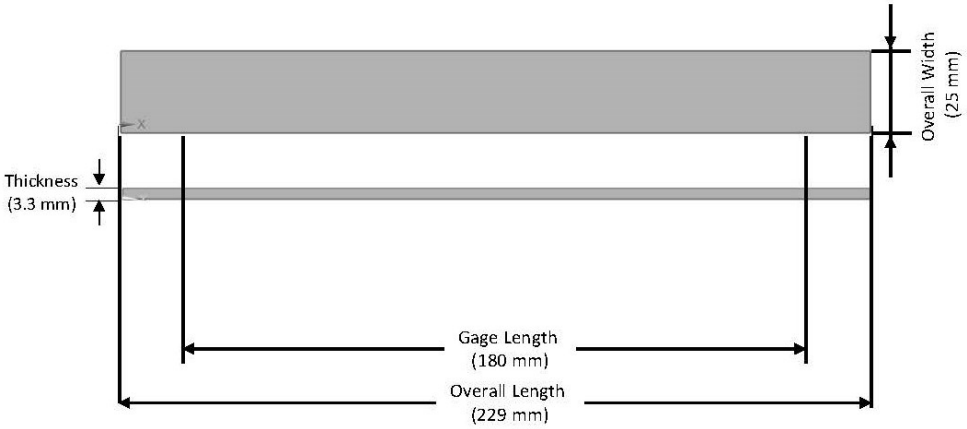

Figure 3. ASTM D3039[3] Rectangular Test Specimen (Dimensions in mm)

The mechanical properties of FFF ABS and other FFF polymers have been extensively studied over the last two decades, evaluating the influence of raster orientation, infill density, layer thickness, number of layers, and air gap on tensile, flexural, compressive, and fatigue behavior.[5; 7-14; 20-22] However, there has been limited published research regarding the rationale for the selection of an ASTM test specimen geometry for FFF polymer materials. Those that do discuss their rationale for selecting an ASTM test specimen geometry do so as a cursory note to the main research.

Ahn, et al.,[14] evaluated the impact of various print parameters including print speed, print temperature, build configuration, extrusion flow, and layer thickness of the rasters on tensile performance of FFF ABS. They compared the performance of the ASTM D638 and ASTM D3039 specimens. They observed that test specimens developed using ASTM D638 Type I dogbone geometry failed by shearing at the fillet radius and hypothesized this was due to stress concentrations in that region. They printed the ASTM Type I dogbone specimens using two different tool paths. However, the ASTM D638 Type I dogbone specimens still exhibited failure at the fillet radius. They hypothesized that both the curvatures in the fibers (tool path 1) and the inconsistent fiber lengths (tool path 2) introduced stress effects at the radius of the dogbone, causing the test specimens to fail outside the gage length. Ahn et al., compared tensile test results from ASTM D638 Type I geometry specimens to ASTM D3039 rectangular geometry specimens and observed that the ASTM D3039 rectangular geometry specimens resolved the issue of failure outside the gage length during testing. Based on this observation, they chose to perform their experimental analysis using the ASTM D3039 rectangular geometry specimens. Ahn et al., did not provide a quantitative comparison of the failure rate between the ASTM D638 Type I and ASTM D3039 geometries.

Rankouhi et al., modified the number of layers of FFF ABS ASTM D638 Type I dogbone specimens to evaluate the impact on tensile performance.[20] They observed that the ASTM D638 Type I dogbone specimens failed at the radius of the dogbone geometry and hypothesized that this was due to stress concentrations, citing the observations of Ahn et al.. Contrary to Ahn et al., they did not choose to change to the ASTM D3039 rectangular geometry. Additionally, the observed that for an increased number of layers (i.e., thicker sample) the tensile performance improved with increases in ultimate tensile strength (UTS) and elastic modulus. This is consistent with the

mechanical behavior of composite materials where the tensile strength is dependent on the number of lamina in the materials.[17; 18]

Croccolo et al., developed an analytical model of the elastic behavior of FFF ABS by evaluating the dimensions, number of contours, and raster angle of the test specimen and compared their model to experimental stress-strain results.[19] As part of their research, Croccolo et al., evaluated the ASTM D638 Type I test specimen geometry. They argued that ASTM D638 Type I geometry was designed for tensile testing of plastics that exhibit isotropic behavior, whereas FFF ABS has been shown to exhibit anisotropic behavior. Therefore, they redesigned the ASTM D638 Type I dogbone geometry by increasing the fillet radius from 76 mm to 244 mm, stating that the change eliminated crack initiation inside the fillet radius. However, they did not specify the failure rate inside the narrow length of the modified Type I test specimens in comparison to the standard ASTM D638 Type I. Furthermore, there was no published information provided about the analysis or results used to determine the selected fillet radius. While they did state that the modified Type I test specimen showed an increase in tensile strength, they did not provide a quantitative comparison of the tensile strength between the modified Type I and the ASTM D638 Type I geometries.

Laureto and Pearce compared the tensile test performance of ASTM D638 Type I and Type IV FFF polylactic acid (PLA) dogbone test specimens for a variety of build parameters including print speed, print temperature, build configuration, extrusion flow, and layer thickness of the rasters.[6] The FFF PLA dogbone test specimens were fabricated using 47 different user assembled 3D printers. They characterized the tensile properties for both Type I and Type IV test specimens. Laureto and Pearce noted that the FFF PLA Type IV test specimens tended to have a higher UTS in comparison to the Type I, but they did not provide any discussion on the cause. Additionally,

they did not discuss any observed failure of the FFF PLA ASTM D638 Type I and Type IV dogbone geometries at or near the fillet radius.

Currently, to the best of our knowledge, there is no published guidance on how to apply ASTM D3039 and ASTM D638 to AM polymers. The goal of the research presented here is to provide evidence-based guidance on the applicability of ASTM D3039 and ASTM D638 on FFF ABS. Existing literature has predominantly focused on the impact FFF print parameters have on the mechanical properties of FFF ABS without placing any significance on the choice of test specimen and test method selected. In contrast, this research evaluated the ASTM D3039 and ASTM D638 Type I and Type IV geometries to determine which test specimen geometry provided the most consistent adherence to the ASTM failure acceptance criteria. Additionally, this research considers how the different geometries impact the tensile test results of FFF ABS. An area for which there is limited information published.

Experimental Study

MATERIALS AND SPECIMENS

All the FFF specimens tested and analyzed in this study were acrylonitrile butadiene styrene (ABS). The FFF ABS test specimens in this study were made of ABS-P430. In general, ABS is a terpolymer that consist of three monomers: acrylonitrile; butadiene; and styrene. The percentage of each monomer in the ABS is specific to the material mixture but can range from 15% to 35% acrylonitrile, 5% to 30% butadiene, and 40% to 60% styrene. The ABS-P430 filament is commercially available but is a proprietary mixture, therefore the exact proportions of each monomer are not publicly available. However, material characterization measurements were conducted on samples printed using the ABS-P430 filament. The results of these tests are presented here in order to provide some insight into the specifics of the ABS filament used in this

study. The material composition of the ABS filament was not varied in this study. The impact of the chemical composition on the results presented in this study were not evaluated.

The molecular weight distribution (MWD) of the FFF ABS was measured by gel permeation chromatography (GPC) using a Waters GPC. The measurements were carried out using tetrahydrafuron (THF) as the solvent and samples were dissolved in THF for 24 hours prior to filtration using a 0.2 μm polytetrafluoroethylene (PTFE) filter. The reflective index was recorded over time and, using EasiCal® wide molecular weight range polystyrene standards, a calibration curve was established from which the peak maxima molecular weight (M_p), number averaged molecular weight (M_n), weighted average molecular weight (M_w), z-averaged molecular weight (M_z), and polydispersity index (PDI) for ABS-P430 were calculated (Table 1).

M_p	82329.67
M_n	71264
M_w	107063.3
M_z	160616.7
M_z/M_w	1.45
PDI	1.49

Table 1. Molecular Weight Distribution of ABS-P430

The decomposition temperature (T_d) of FFF ABS was measured by thermogravimetric analysis (TGA) on a Seiko Instruments TGA/DTA320 machine using an inert N_2 gas atmosphere of at 150 cm^3/min in a two-step heating cycle. Step one consisted of a heating rate of 10°C min^{-1} from 25°C to 100°C. Step two consisted of a heating rate of 5°C min^{-1} from 100°C to 550°C. The T_d at 5% decomposition was 365.81°C ± 1.54°C.

The chemical composition of the FFF ABS was measured by infrared spectroscopy using a Bruker Fourier transform infrared spectroscopy (FTIR) with attenuated total reflection (ATR). FTIR spectra is provided in Figure 4. Table 2 provides a comparison of the wavenumbers and

percent transmittance (%T) for the peaks of significance. The peaks of significance are based on published literature for ABS.[23]

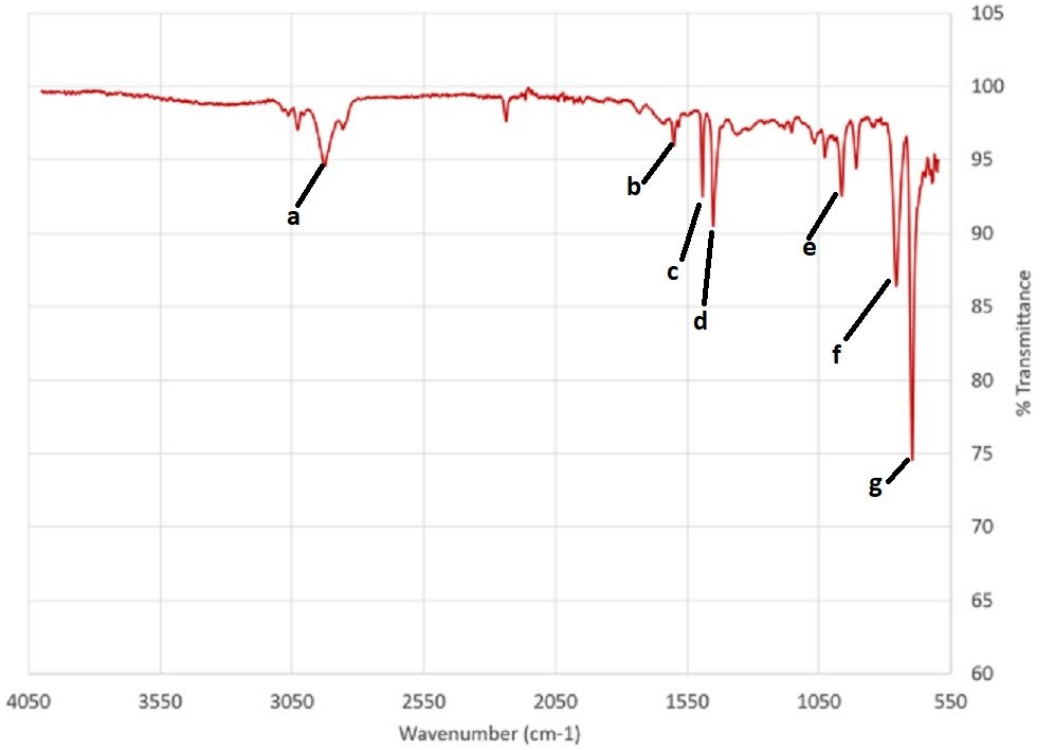

Figure 4. ABS P430 FTIR Spectra

	Wavenumber (cm^{-1})	**Assignment[23]**	**%T**
a	2925.2	C-H stretch	94.5
b	1602.2	Aromatic ring stretch	94.1
c	1493.8		92.7
d	1452.6	CH2 bend	90.7
e	966.0	=C-H bend	92.9
f	758.8	Aromatic CH out-of-plane bend, =CH bend	87.2
g	698.7	Aromatic CH out-of-plane bend	76.9

Table 2. ABS-P430 FTIR Peaks of Significance

All test specimens were built to a nominal thickness of 3.3 mm. FFF ABS test specimens were built on a Dimension 1200es SST and uPrint FFF printers. Solid models were created using commercially available CAD software and exported as stereolithography (STL) files. The STL files were uploaded to a commercially available slicing software and printed. As stated in the literature review, researchers primarily use FFF ABS test specimens that conform to either the ASTM D638 Type I or ASTM Type IV dimensions. Therefore, the Type I and Type IV dogbone-shaped test specimens (Figure 1 and Figure 2) were used in this study in accordance with the requirements of ASTM D638. The fillet radius for ASTM D638 Type I and radii for ASTM D638 Type IV are below the narrow length and above the grip. In this study a failure in the fillet is any failure that occurred above the grip but below the narrow length section.

ASTM D3039 requires that the length of a composite polymer test specimen be a minimum length equal to the sum of the grip length, twice the width, and the gage length, where the gage length is the overall length minus the grip length. The recommended width for a balanced and symmetric fiber composite is 25 mm. The width and the thickness should be "large enough to promote failure in the gage length and contain enough fibers to be statistically representative of the bulk material."[3] The recommended dimensions in ASTM D3039 have been "found through numerous testing at laboratories to produce acceptable failure modes for a wide variety of material systems, but use of them does not guarantee success for every existing future material.[3]" Figure 3 details the dimensions for the rectangular specimens and provides a schematic. According to ASTM D3039 any portion of the rectangular specimen not inside the grips is the gage length.[3] Since the ASTM D3039 test specimen is a rectangular geometry, there is no section called the "narrow length" in contrast to the ASTM D638 Type I and IV dogbone specimens.

Test specimens were made using the build parameters outlined in Table 3 and only build parameters that were available to the user for modification are considered. The Solid and Sparse High Density infills are FFF printer specific options provided in the slicing software and are used instead of a manually selected infill percentage. The Solid infill provides the least amount of spacing between the rasters. The Sparse High Density provides slightly greater spacing between the rasters. Additionally, the FFF printer used in this study does not support manually varying parameters such as air gap, nozzle temperature or speed, build platform temperature, or environment temperature. Existing literature on FFF ABS and other FFF polymers has evaluated the variations in infill density percentage, layer resolution, air gap, nozzle speed, temperature, and material color with mechanical performance. This study focuses on the impact of test specimen geometry to determine which test specimen geometry provides the most consistent adherence to the ASTM failure acceptance criteria. Additionally, this research considers how the different geometries impact the tensile test results of FFF ABS. Therefore, variations in build parameters were considered only in relation to how each geometry responded in adherence to failure criteria and to confirm any trends observed in tensile test results. Each test specimen was built in a flat build orientation.

Build Number	Raster Orientation	Layer Resolution	Fill Density
1	45°/-45°	0.2540 mm	Solid
2	45°/-45°	0.3302 mm	Solid
3	45°/-45°	0.2540 mm	Sparse High Density
4	45°/-45°	0.3302 mm	Sparse High Density
5	0°/90°	0.2540 mm	Solid
6	0°/90°	0.3302 mm	Solid
7	0°/90°	0.2540 mm	Sparse High Density
8	0°/90°	0.3302 mm	Sparse High Density

Table 3. Build Parameter Combinations for Each Test Specimen Geometry

A comparison was made between samples printed on the Dimension and samples printed on the uPrint. Due to the limitations of the uPrint (i.e., only 0.254 mm layer resolution available and smaller build platform) only builds 1, 2, 5, and 7 for the ASTM D638 Type IV and Type I specimen geometries were printed on both printers. ASTM D3039 specimen geometry was only made on the Dimension due to the overall size of the specimen, which exceeded the build platform dimensions of the uPrint. There was no statistically significant difference in the UTS and elastic modulus when comparing samples printed on only the Dimension or only the uPrint to the sample set tested in this study. Additionally, there was no statistically significant difference in the percentage of adherence to failure criteria for specimens that were printed only on the Dimension or only on the uPrint to the sample set tested in this study. No samples broke inside the grip during testing.

ASTM D638 dogbone geometries used in this study have discontinuities as the printer generates the specimen's filled radius. Figure 5 shows the location of these fillets and the raster length discontinuities in the ASTM D638 Type I test specimen geometry. Similar discontinuities exist in the ASTM D638 Type IV geometry at the grip-fillet and fillet-narrow length interfaces. How pronounced these discontinuities are is a function of the raster orientation chosen and the test specimen geometry selected. It has been shown in prior studies that these discontinuities have contributed to failure outside of the gage length.[13; 14; 20] The smaller radius of the Type IV dogbone geometry is complimented by an interior fillet that provides a smoothed transition from the grip to the gage. This feature is lacking in the ASTM D638 Type I geometry. The ASTM D3039 rectangular test specimen has no fillet radius and therefore the raster lengths are equivalent throughout out the body of the specimen based on the raster orientation selected.

(a) (b)

Figure 5. Raster Discretization at Fillet Radius for: (a) ASTM D638 Type I 45°/-45° Raster orientations; and (b) ASTM D638 Type I 0°/90° Raster orientations.

EXPERIMENTAL DESIGN

Tensile tests were performed on an Instron model 5569A dual column uniaxial material testing machine with 0.02 mm displacement precision, up to 0.002 N force accuracy, and 50 kN load capacity. Samples of all geometries were manually secured in the jaws of mechanical wedge action grips. During preliminary testing, no slippage was observed at the grips; therefore, no tabs were used on the grips of the specimens, in accordance with the guidance of ASTM D638 and D3039. The samples were marked to indicate orientation on the testing machine (i.e., which side of the sample was secured to the bottom load cell). Five (5) samples were tested per build, as outlined in Table 3 (i.e., 8 builds). Testing was performed for all three (3) geometries evaluated in this study (i.e., ASTM D638 Type I, Type IV, and ASTM D3039) for a total of 120 (i.e., 5 x 8 x 3) samples tested. Tensile tests were run at test speeds provided in Table 4, in accordance with the recommendations of ASTM D638 and ASTM D3039. Force was applied to along the longitudinal axis until fracture occurred. The average tensile properties of samples (UTS, elastic modulus, and yield stress) were calculated.

Following fracture, each sample was measured to determine the location of fracture. In order to determine the failure point, the position of the testing machine grips was marked on all

samples with an arrow pointing in the direction of the moving grip. The bottom and top of each sample was labeled with the specimen number and build group and fractured samples were maintained together after testing. The bottom portion of each sample was measured to the fracture surface and the average of the highest and lowest point of the fractured surface was taken as the point of failure. Specimen's failure position was then assessed using respective ASTM defined geometry dimensions to determine compliance failure acceptance criteria. More specifically, successful mechanical performance as denoted in the ASTM test standards requires failure inside the narrow length or outside of the grips. For ASTM D638 Type I and Type IV dogbone geometry specimens the failure point was compared to the ASTM D638 defined narrow length position (See Figure 1 and Figure 2, respectively) to determine acceptability. Samples that broke inside the fillet (i.e., above the grip and below the ASTM D638 defined narrow length) were evaluated as not in compliance with the ASTM D638 failure acceptance criteria. For ASTM D3039 test specimens, the failure point was compared to the gage length (See Figure 3) to determine compliance. Samples that broke at or inside the grip were evaluated as not in compliance with the ASTM D3039 failure acceptance criteria. The percent adherence to ASTM failure criteria was determined by the ratio of samples in a build that satisfied the ASTM failure criteria to the total number of samples tested per build. Five samples were tested per build for each geometry to evaluate the ability of each geometry to satisfy the failure acceptance criteria.

Test Specimen Geometry	Test Speed (mm/min)
ASTM D638 Type I	5
ASTM D638 Type IV	5
ASTM D3039 Rectangular	2

Table 4. Test Speed for ASTM D638 and ASTM D3039 Tension Test

Results and Discussion

ADHERENCE TO FAILURE CRITERIA

As described in the experimental design section, ASTM D638 Type I, ASTM D638 Type IV and ASTM D3039 geometry samples underwent uniaxial tensile testing until fracture was achieved and their percent adherence to respective failure criteria were recorded. Table 5 lists the percent of samples that adhered to the ASTM failure acceptance criteria as described in the Experimental Design section. Figure 6, Figure 7, and Figure 8 provide scatter plots of the sample failure point locations of each sample tested for each build and each specimen geometry. All samples, including samples that did not satisfy the ASTM acceptance criteria, were included in the figures. The failure points in relation to the areas of the specimen (i.e., grip, narrow length, or fillet) are described in the figures. In some cases, multiple specimens broke in the same fillet location, which gives the appearance of less than five samples per build.

Build Number	Type IV	Type I	D3039
1	60%	80%	100%
2	80%	100%	100%
3	40%	40%	100%
4	100%	100%	100%
5	100%	20%	100%
6	60%	100%	80%
7	80%	20%	100%
8	40%	40%	80%

Table 5. Comparison of Test Specimen Failure Performance in the Narrow Length (ASTM D638) or Gage Length (ASTM D3039)

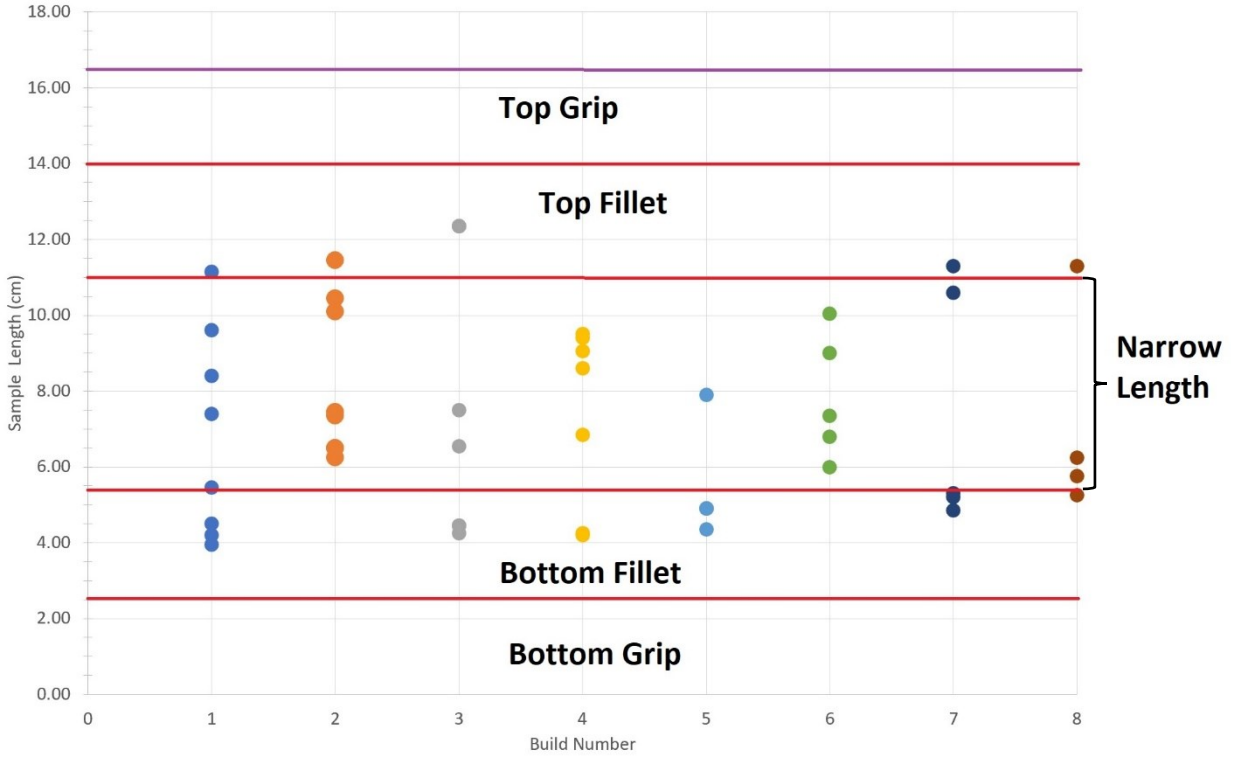

Figure 6. ASTM D638 Type I Dogbone Geometry Samples Break Location

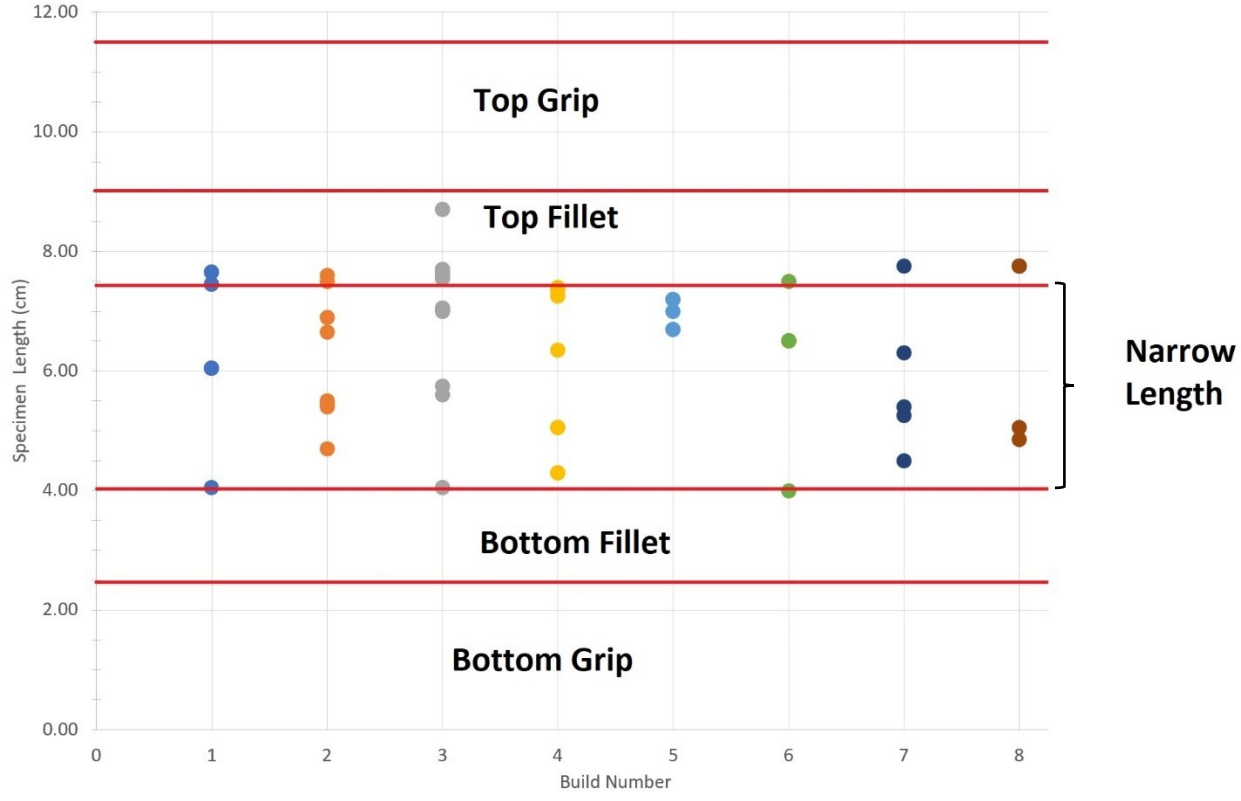

Figure 7. ASTM D638 Type IV Dogbone Geometry Samples Break Location

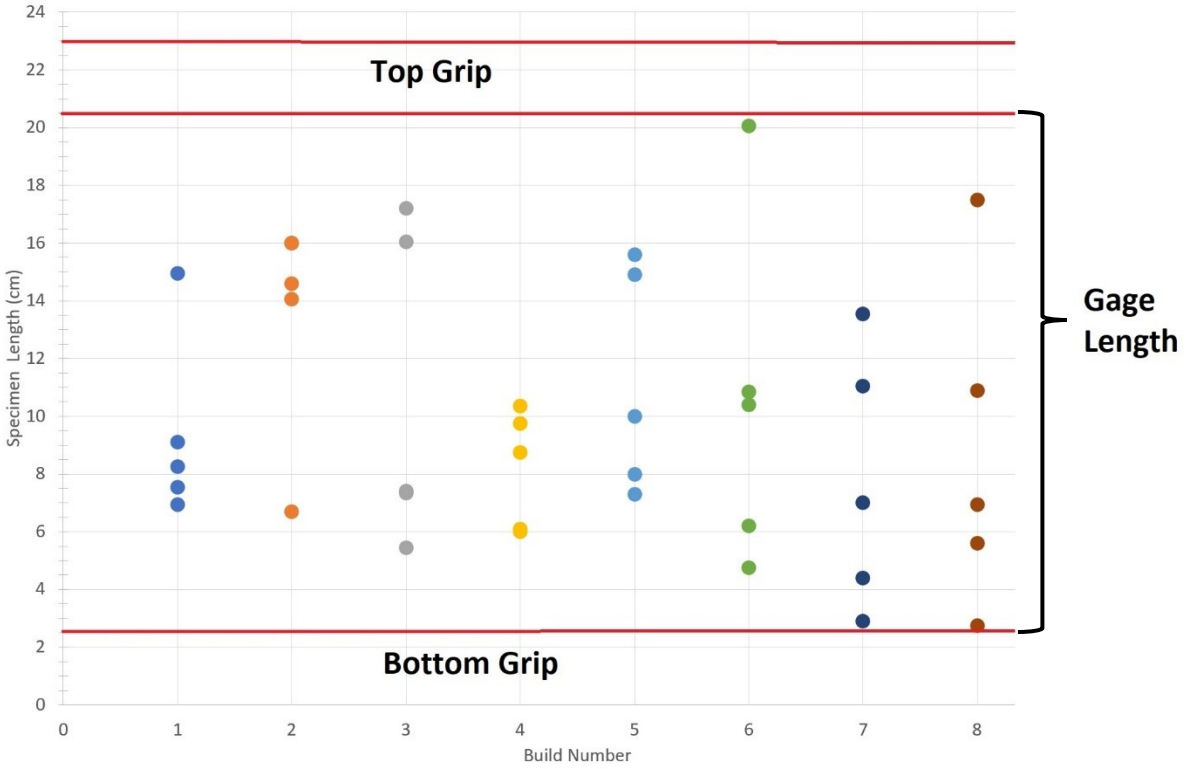

Figure 8. ASTM D3039 Rectangular Specimen Geometry Samples Break Location

ASTM D638 dogbone geometry specimens exhibited a susceptibility to failure within the fillet radius caused by discontinuities in the raster length as the specimen transitioned from the grip to the narrow length. Figure 9 shows the failure of the Type I and Type IV test specimens outside the narrow length (i.e., above the grip height and below the ASTM D638 defined narrow length). No ASTM D638 Type I or Type IV samples broke inside the grip during testing. The ASTM D3039 rectangular geometry specimens consistently broke inside the gage length and satisfied the ASTM D3039 failure criterion. On two occasions, once in for build 6 and once for build 8, the D3039 samples broke inside the grip. Per ASTM D3039 guidance, specimens that preferentially break inside the grip should have tabs added to the them. No tabs were used during this study to test the ASTM D3039 geometry samples due to the limited number of samples that broke inside the grip.

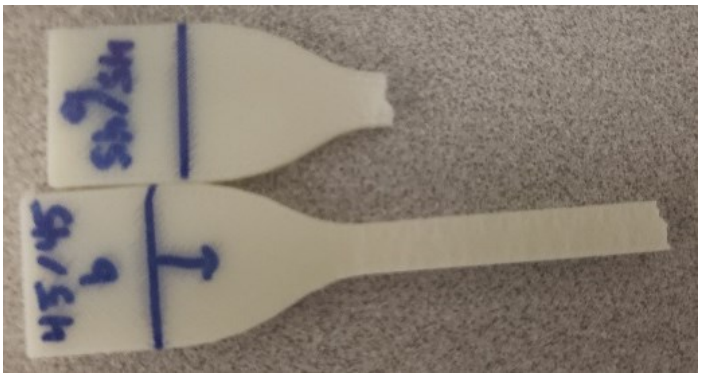

(a)

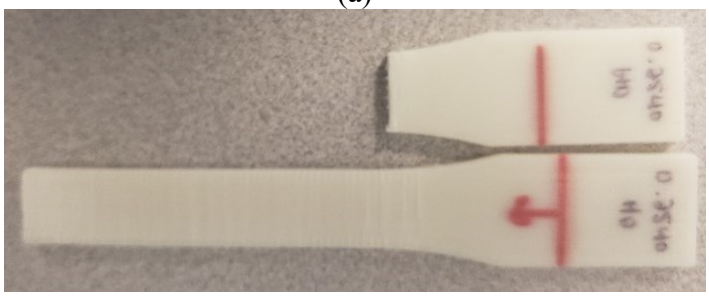

(b)

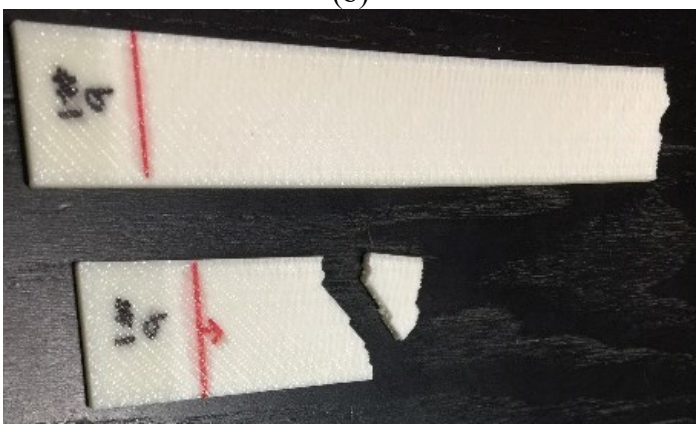

(c)

Figure 9. Test Specimen Geometries Tensile Failure: (a) ASTM D638 Type IV, Build 3, Failure at Outside Narrow Length; (b) ASTM D638 Type I, Build 7, Failure Outside Narrow Length; and (c) ASTM D3039, Build 3, Failure Inside Gage Length.

ASTM D638 Type IV and Type I dogbone geometry specimens inconsistently satisfied the ASTM D638 failure acceptance criterion. Only builds 4 and 5 had 100% for Type IV geometry and builds 2, 4, and 6 for Type I geometry complied with failure acceptance criterion. For these builds all five specimens tested broke within the narrow length of the dogbone. The Type IV percent compliance never dropped below 40% for all builds. For the Type I geometry builds 5

and 7 only achieved 20% compliance. The Type IV geometry has a shorter and narrower narrow length and has a smaller fillet radius. Additionally, the inner fillet of the Type IV specimens provides a smoother transition from the grip into the narrow length reducing the effects of stress concentrations due to raster length discontinuities. The Type I geometry only has one fillet radius between the grip and narrow length and therefore cannot benefit from this feature.

ASTM D3039 rectangular geometry specimens performed best across all builds with respect to failure acceptance criterion in comparison to the ASTM D638 Type I and Type IV geometries. For the ASTM D3039 rectangular geometry, only builds 6 and 8 had failures outside of the gage length. Overall, the ASTM D3039 rectangular geometry specimens, across all builds, was 95% compliant with the ASTM D3039 failure acceptance criterion. These results can be attributed to the rectangular structure of the geometry. Abrupt changes in geometry can give rise to stress concentrations in an FFF manufactured part. The intent of the curved radii integrated into dogbone specimen design is to drive the concentration of stress into the gage length, regardless of various imperfections and inclusions found in the bulk. Although this technique is effective for a continuum of ductile material, this only serves to exacerbate localized stress concentrations found in FFF manufactured parts, such as the discretization of individual filament rasters at fillet radii. Therefore, the stress concentrations at the radius of the ASTM D638 Type I and IV geometries led to increased failure rates, while the absence of the fillet radius in the ASTM D3039 rectangular geometry yielded more compliant test results.

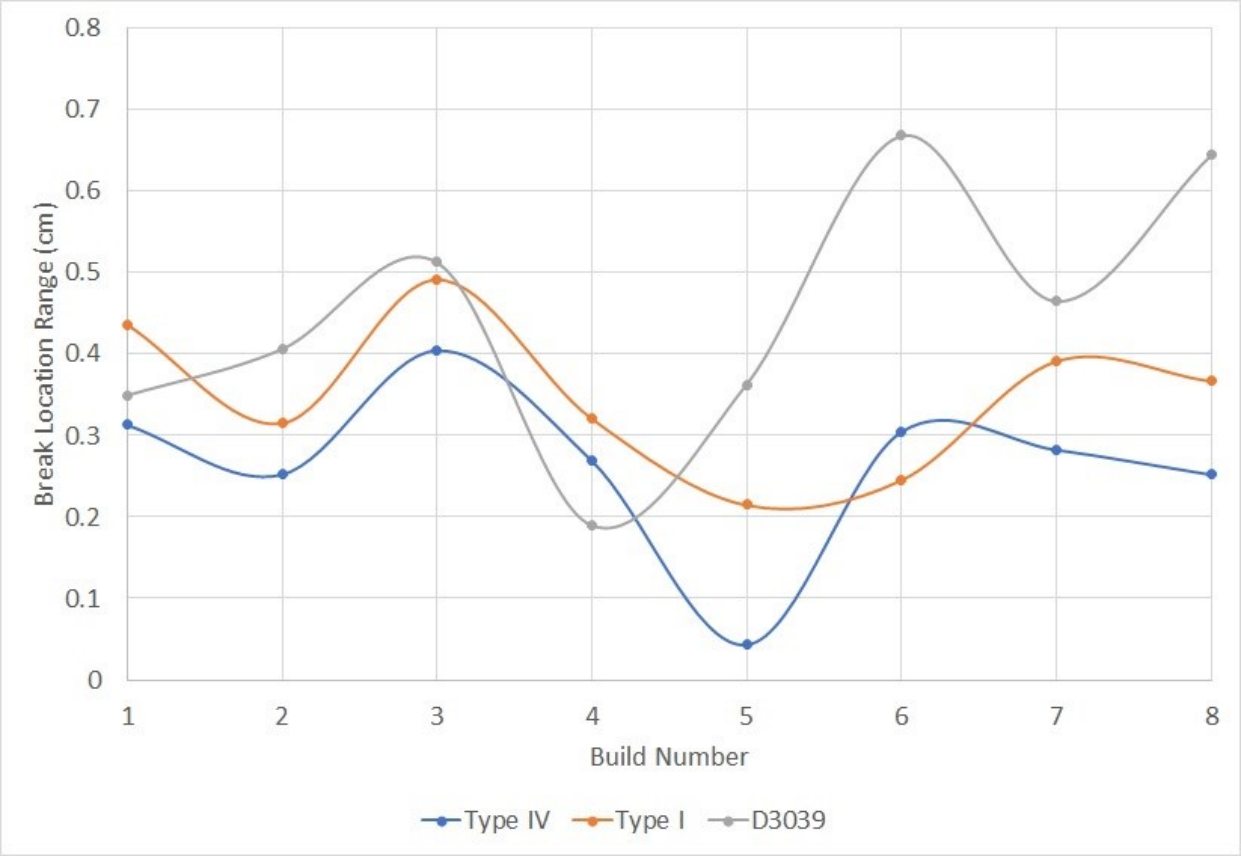

Figure 10. Beak Location Normalized to Test Geometry Overall Length for all Builds

Across the three test geometries, observations were noted in relation to the range of break locations across the different builds, where the range is defined as the difference between the highest and lowest break points. Figure 10 is a plot of the break location ranges of each build normalized to the overall length of the respective test geometry. As shown in Figure 10, the ASTM D638 test geometries exhibit a similar trend across all builds. However, ASTM D3039 test geometry does not obey the same trend.

EFFECT OF ADHERENCE TO FAILURE CRITERIA ON TENSILE TEST RESULTS

A comparison of mean UTS was made between two sample sets. The first set included five consecutively tested specimen regardless of failure within the narrow length. The second set only included test samples that met the ASTM D638 acceptance criteria. For Type I and IV specimens with builds that did not have 100% of specimens tested break inside the narrow length (see Table 5), additional testing was performed until a total of five samples[e] failed inside the narrow length for both the ASTM D638 Type I and Type IV test specimens.[f] The results indicate slightly higher mean UTS values for most build configurations when all five samples successfully failed within the narrow length. Figure 11 show no statistical difference in mean UTS between samples that only failed inside the narrow length to samples that either failed inside or outside of the narrow length. The results of the mean elastic modulus (Figure 12) show some builds exhibiting statistically significant differences by exceeding one standard deviation.

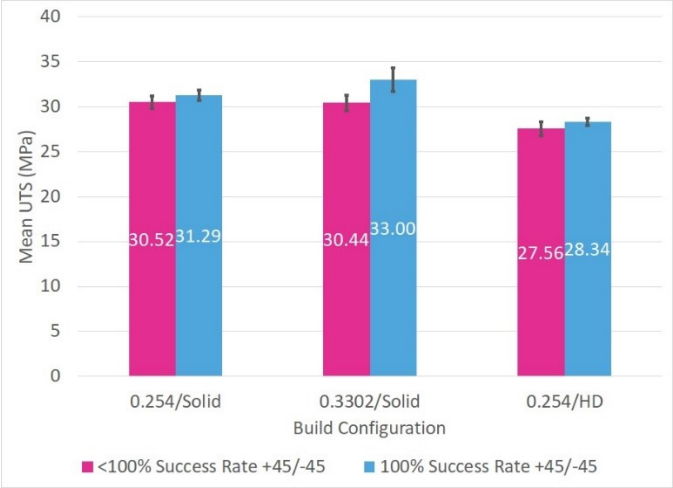

(a)

[e] This is in addition to the 120 total samples initially tested to compile the data in Table 5.
[f] Note that for Type I 0°/90° builds 0.254 mm Solid and HD, only 4 replicates out of 25 broke inside the narrow length for the 100% Success Rate and therefore the Mean UTS and standard deviations for those builds are based on four samples. All others are based on five samples.

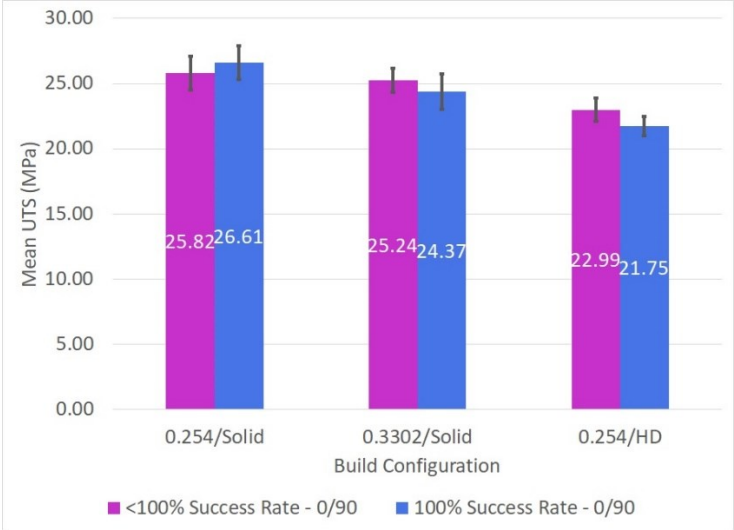

(b)

Figure 11. Comparison of Mean UTS for ASTM Type IV Geometry Sample Sets with 100% Failure Inside Narrow Length and < 100% Failure Inside Narrow Length: (a) 45°/-45° Raster Orientation Builds 1 – 3; (b) 0°/90° Raster Orientation Builds 6 – 8.

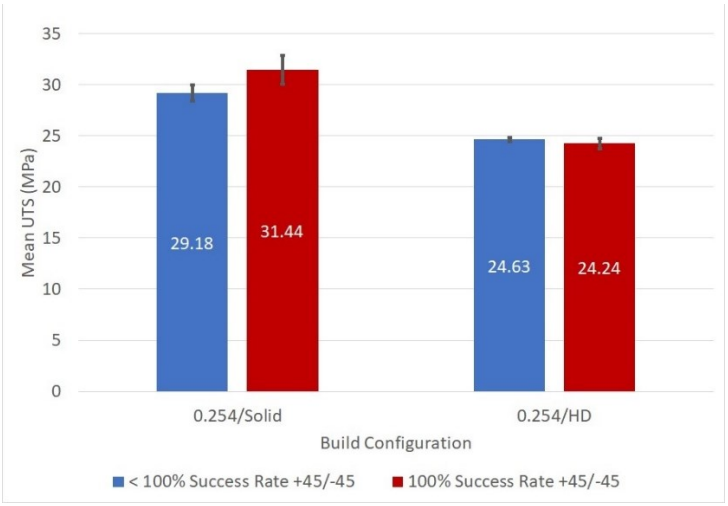

(a)

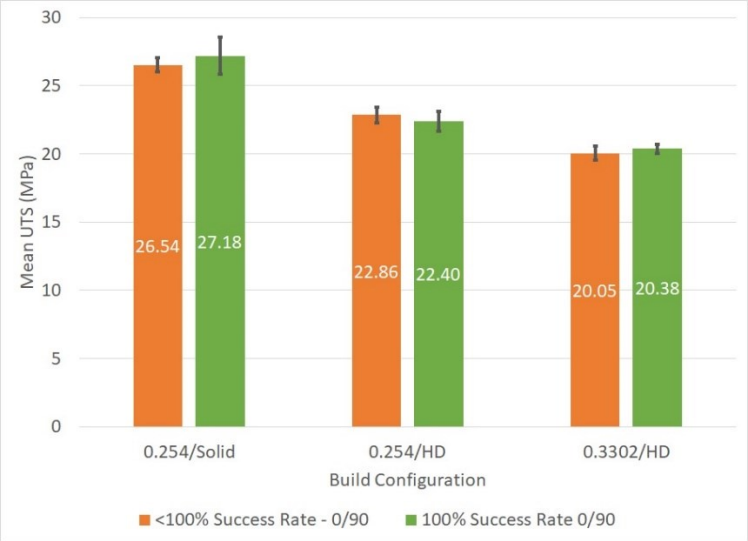

(b)

Figure 12. Comparison of Mean UTS for ASTM Type I Geometry Sample Sets with 100% Failure Inside Narrow Length and < 100% Failure Inside Narrow Length: (a) 45°/-45° Raster Orientation Builds 1 and 3; and (b) 0°/90° Raster Orientation Builds 5, 7 and 8.

EFFECTS OF GEOMETRY ON TENSILE PERFROMANCE

The trend of mean UTS and elastic modulus for all three test specimen geometries was plotted in Figure 13 and Figure 14for build parameters. The figures show that irrespective of build, the mean UTS and elastic moduli increase with respect to specimen geometry. This is due to the difference in cross-sectional area of the gage length between the three geometries (Table 6). The difference in the cross-sectional area between the three test specimen geometries is due to the difference in gage length width. As the cross-sectional areas of the gage length decreases, the mean UTS increases for the same build.

Test Specimen Geometry	Nominal Cross-Sectional Area of Gage Length (mm^2)	Gage Length Width (mm)
ASTM D638 Type IV	19.8	6
ASTM D638 Type I	42.9	13
ASTM D3039 Rectangular	82.5	25

Table 6. ASTM Test Specimen Geometry Gage Length Width and Cross-Sectional Area

The ASTM D638 Type IV test specimen geometry overestimates UTS but underestimates elastic modulus. Conversely, the ASTM D3039 test specimen geometry overestimates elastic modulus but underestimates UTS. The ASTM D638 Type I test specimen geometry performed midway between the Type IV and D3039 for both UTS and elastic modulus. Laureto and Pearce observed similar behavior when comparing ASTM D638 Type IV and Type I test specimen geometries using PLA, however they did not expand on the observation.[6]

Classical laminar theory (CLT) is a commonly used method for modeling the orthotropic behavior of composite materials. In CLT the elastic behavior of a unidirectional lamina, or raster in FFF, is used to create the stiffness matrix and derive the stresses exerted on a composite part consisting of cross-ply lamina. These unidirectional properties will vary based on raster orientation (i.e., ply direction) and dimensions of the test specimen. Cross-ply raster orientations are derived from unidirectional raster orientation component elastic properties. Stress is calculated from the derived stiffness matrix and strains. The strains are calculated from matrices that are a function of the stiffness matrix and the distances from the midplane for each lamina in the part.

While traditionally manufactured ABS behaves isotropically, FFF ABS behaves orthotropically due to the composite nature of the mesostructure. The elastic modulus of composite materials will vary with changes in geometry as well as ply orientation (e.g., raster orientation). Rodriguez and Li separately studied the orthotropic behavior of FFF ABS and found that CLT adequately modeled FFF ABS tensile performance. Rodriguez observed that CLT could be used to model FFF ABS.[18] Li expanded on the work of Rodriguez and refined the CLT model to address the presence of air gaps in FFF ABS parts, a feature unique to the FFF printing process.[15] She found that accounting for the air gap in the CLT model provided a better fit of experimental

data to the theoretical model. Based on existing literature, the differences in UTS and elastic modulus between the three test geometries, observed in this study, is a result of the orthotropic behavior of the parts resulting from the FFF process.

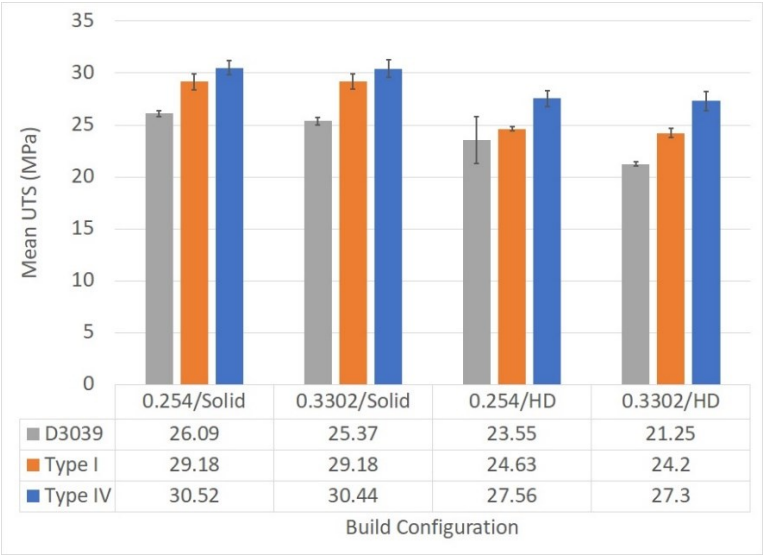

(a)

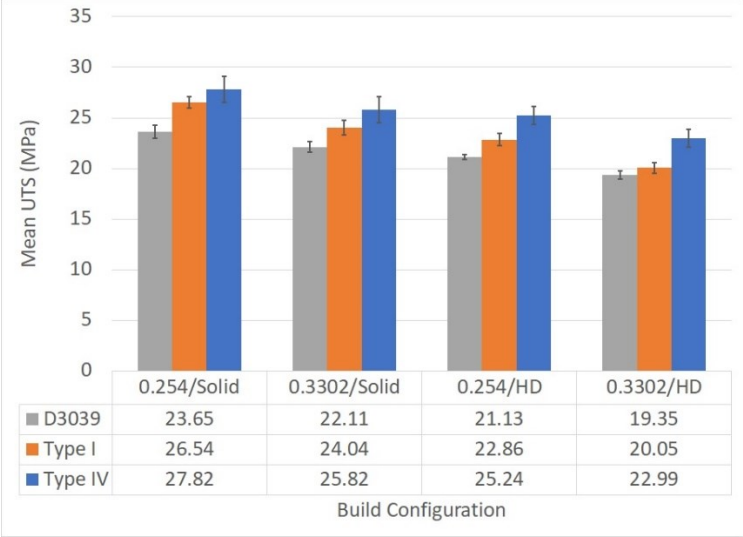

(b)

Figure 13. Mean UTS (MPa) for ASTM D638 Type I and IV and ASTM D3039 Test Specimens: (a) Builds 1-4; and (b) Builds 5-8

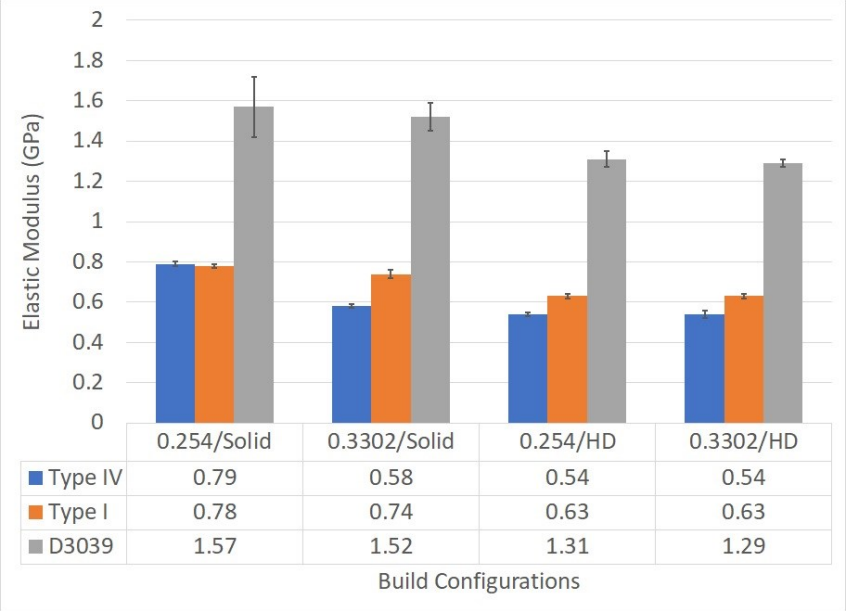

(a)

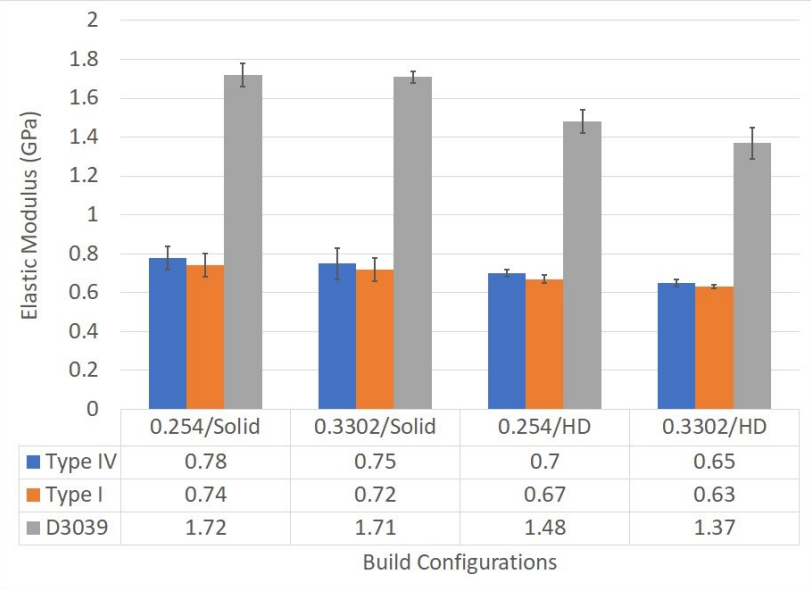

(b)

Figure 14. Mean Elastic Modulus (GPa) for ASTM D638 Type I and IV and ASTM D3039 Test: (a) Builds 1-4; and (b) Builds 5-8

Conclusion and Future Work

The results of this study show there is inherent benefit to using ASTM D3039 over ASTM D638 test specimen geometries for tensile testing when considering adherence to ASTM failure acceptance criteria. The ASTM D3039 rectangular test specimen consistently adhered to ASTM

D3039 stated failure acceptance criteria across all builds. ASTM D638 Type I and Type IV test specimen geometries performed inconsistently. ASTM D3039 rectangular samples provide a relatively higher elastic modulus and relatively lower UTS in comparison to ASTM D638 geometries. The ASTM D638 standard does provide for the testing of reinforced composite materials through the Type I specimen. However, based on the results of this study, the ASTM D3039 rectangular test specimen provided consistently valid test results over a set sample size. That is, irrespective to build, the ASTM D3039 rectangular specimen, consistently adhered to the test method's stated failure acceptance criterion. Therefore, depending on the build parameters being tested, it is more likely that, for ASTM D638 test geometries, more than five samples will be required to achieve a minimum of five samples failing inside the narrow length. The ASTM D3039 rectangular test specimen has a higher likelihood of meeting the sampling requirement with fewer replicates tested. Given the composite mesostructure of FFF ABS, the ASTM D3039 rectangular specimen should provide the most accurate tensile results as the ASTM D3039 test method is relevant to composite materials with rasters that are balanced and symmetric to the load. Neither the ASTM D3039 nor the ASTM D638 standards are specifically written for polymers manufactured using FFF. Until further ASTM guidance and standards are released specific to FFF polymers, it is the assessment of this study that ASTM D3039 is better suited for tensile testing of FFF ABS.

While the difference in failure acceptance percentage between ASTM test geometries was evaluated in this study, a difference in the randomness of the break location was also observed. The randomness of the break locations increased with the length of the test specimen geometry due to an increase in potential crack nucleation sites. The amount of randomness differed for the same build across the three test geometries, however similarity in the randomness of build 5 for

the ASTM D638 geometries was observed. The difference between the highest and lowest break locations per build was similar across the ASTM D638 geometries. However, the same trend was not observed in the ASTM D3039 rectangular specimen samples. These observations led the authors to conclude that no major repeated defect was introduced to the samples by the FFF printers. However, further investigation into such variation among samples is warranted.

Some advantages of using the ASTM D638 Type I and IV specimens over the ASTM D3039 rectangular specimen are print time and relative size. During this study it took six hours to print eight ASTM D3039 test specimens. In comparison, it took the same amount of time to print 22 ASTM D638 Type IV specimens or 13 ASTM D638 Type I in the same printer. Therefore, even though it may require testing more than five ASTM D638 samples to achieve statistically valid results, more samples are available for testing per print batch. Additionally, as stated in the Introduction, most existing literature on FFF ABS tensile performance uses ASTM D638 Type I or IV test specimen geometries. Testing using the ASTM D638 geometries allows for better comparison of experimental results to published data. This assumes all print parameters, filament choice, and printer selection are considered when comparing results.

Overall, any of the three test specimen geometries can be utilized for testing FFF ABS, but the ASTM D3039 test specimen adherence to failure acceptance criteria is more consistent than the ASTM D638 test geometries. The ASTM D3039 standard accounts for the unique aspects of composite material performance, which more closely aligns with the mechanical performance of FFF ABS.

Future study will focus on the impact test specimen geometry has on fatigue performance. Additional investigation into the effect of builds parameters on the randomness of break location is also warranted. Finally, the effect of printer reliability and repeatability on test results was not

evaluated in this study and should be investigated further as it relates to adherence to ASTM failure acceptance criteria.

ACKNOWLEDGMENTS

The authors gratefully acknowledge the financial support of Consortium for Advanced Manufacturing. The contributions of Dr. Lori Tunstall (KCP), Dr. John Abrefah (DNFSB), Dr. Kalman Migler (NIST), and Dr. Gbadebo Owolabi (Howard University) for advice and helpful discussion. The authors gratefully acknowledge the support of Dr. Gbadebo Owolabi (Howard University) for the use of his testing equipment during this study.

References

1. Forster, A. M., *Materials Testing Standards for Additive Manufacturing of Polymer Materials: State of the Art and Standards Applicability,* National Institute of Standards and Testing, NISTIR 8059, (Gaithersburg, MD: NIST) (2015).
2. ASTM International, *Standard Test Method for Tensile Properties of Plastics,* ASTM D638, (2014).
3. ASTM International, *Standard Test Method for Tensile Properties of Polymer Matrix Composite Materials,* ASTM D3039, (2017).
4. Migler, K. B., "NIST Releases Roadmap for Polymer-Based Additive Manufacturing," National Institute of Standards and Technology. Accessed October 26,. https://www.nist.gov/news-events/news/2016/12/nist-releases-roadmap-polymer-based-additive-manufacturingd.
5. Es-Said, O. S., Foyos, J., Noorani, R., et al., "Effect of Layer Orientation on Mechanical Properties of Rapid Prototyped Samples," *Materials and Manufacturing Processes* 15 (1), 107-122 (2000). https://doi.org/10.1080/10426910008912976.
6. Laureto, J. J., and Pearce, J. M., "Anisotropic mechanical property variance between ASTM D638-14 type i and type iv fused filament fabricated specimens," *Polymer Testing* 68, 294-301 (2018). https://doi.org/10.1016/j.polymertesting.2018.04.029.
7. Lee, B. H., Abdullah, J., and Khan, Z. A., "Optimization of rapid prototyping parameters for production of flexible ABS object," *Journal of Materials Processing Technology* 169 (1), 54-61 (2005). https://doi.org/10.1016/j.jmatprotec.2005.02.259.
8. Lee, C. S., Kim, S. G., Kim, H. J., et al., "Measurement of anisotropic compressive strength of rapid prototyping parts," *Journal of Materials Processing Technology* 187-188, 627-630 (2007). https://doi.org/10.1016/j.jmatprotec.2006.11.095.
9. Letcher, T., Rankouhi, B., and Javadpour, S., "Experimental Study of Mechanical Properties of Additively Manufactured ABS Plastic as a Function of Layer Parameters,"

International Mechanical Engineering Congress and Exposition, Houston, TX, November 13-19, 2015.
10. Sood, A. K., Ohdar, R. K., and Mahapatra, S. S., "Parametric Appraisal of Mechanical Property of Fused Deposition Modelling Processed Parts," *Materials & Design* 31 (1), 287-295 (2010). https://doi.org/10.1016/j.matdes.2009.06.016.
11. Sood, A. K., Ohdar, R. K., and Mahapatra, S. S., "Experimental investigation and empirical modelling of FDM process for compressive strength improvement," *Journal of Advanced Research* 3 (1), 81-90 (2012). https://doi.org/10.1016/j.jare.2011.05.001.
12. Ziemian, C. W., Ziemian, R. D., and Haile, K. V., "Characterization of stiffness degradation caused by fatigue damage of additive manufactured parts," *Materials & Design* 109, 209-218 (2016). https://doi.org/10.1016/j.matdes.2016.07.080.
13. Ziemian, C. W., Ziemian, S., and Sharma, M., "Anisotropic mechanical properties of ABS parts fabricated by FDM," *Mechanical Engineering*InTech Open (2012). https://doi.org/10.5772/34233. https://www.intechopen.com/books/mechanical-engineering/anisotropic-mechanical-properties-of-abs-parts-fabricated-by-fused-deposition-modeling-.
14. Ahn, S. H., Montero, M., Odell, D., et al., "Anisotropic material properties of fused deposition modeling ABS," *Rapid Prototyping Journal* 8 (4), 248-257 (2002). https://doi.org/10.1108/13552540210441166.
15. Li, L., "Analysis and Fabrication of FDM Prototypes with Locally Controlled Properties," Doctorate of Philosophy Dissertation, Department of Mechanical and Manufacturing Engineering, University of Calgary (2002).
16. Li, L., Sun, Q., Bellehumeur, C., et al., "Composite Modeling and Analysis of FDM Prototypes for Design and Fabrication of Functionally Graded Parts."
17. Li, L., Sun, Q., Bellehumeur, C., et al., "Composite Modeling and Analysis for Fabrication of FDM Prototypes with Locally Controlled Properties," *Journal of Manufacturing Processes* 4 (2), 129-141 (2002). https://doi.org/10.1016/s1526-6125(02)70139-4.
18. Rodriguez-Matas, J. F., "Modeling The Mechanical Behavior Of Fused Deposition Acrylonitrile-Butadiene-Styrene Polymer Components," Doctor of Philosophy, Mechanical Engineering, University of Notre Dame (1999).
19. Croccolo, D., De Agostinis, M., and Olmi, G., "Experimental Characterization and Analytical Modelling of the Mechanical Behaviour of Fused Deposition Processed Parts Made of ABS-M30," *Computational Materials Science* 79, 506-518 (2013). https://doi.org/10.1016/j.commatsci.2013.06.041.
20. Rankouhi, B., Javadpour, S., Delfanian, F., et al., "Failure Analysis and Mechanical Characterization of 3D Printed ABS With Respect to Layer Thickness and Orientation," *Journal of Failure Analysis and Prevention* 16 (3), 467-481 (2016). https://doi.org/10.1007/s11668-016-0113-2.
21. Rodríguez, J. F., Thomas, J. P., and Renaud, J. E., "Mechanical behavior of acrylonitrile butadiene styrene (ABS) fused deposition materials. Experimental investigation," *Rapid Prototyping Journal* 7 (3), 148-158 (2001). https://doi.org/doi:10.1108/13552540110395547.
22. Rodríguez, J. F., Thomas, J. P., and Renaud, J. E., "Mechanical behavior of acrylonitrile butadiene styrene fused deposition materials modeling," *Rapid Prototyping Journal* 9 (4), 219-230 (2003). https://doi.org/doi:10.1108/13552540310489604.

23. Jung, M. R., Horgen, F. D., Orski, S. V., et al., "Validation of ATR FT-IR to identify polymers of plastic marine debris, including those ingested by marine organisms," *Mar Pollut Bull* 127, 704-716 (2018). https://doi.org/10.1016/j.marpolbul.2017.12.061.

List of Figures